

Structure and stability of small H clusters on graphene

Željko Šljivančanin,^{1,2} Mie Andersen,¹ Liv Hornekær,¹ and Bjørk Hammer¹

¹*Interdisciplinary Nanoscience Center (iNANO) and Department of Physics and Astronomy,
Aarhus University, Ny Munkegade 120, building 1520, DK-8000 Århus C, Denmark*

²*Vinča Institute of Nuclear Sciences (020), P.O.Box 522, RS-11001 Belgrade, Serbia*
(Dated: January 13, 2013)

The structure and stability of small hydrogen clusters adsorbed on graphene is studied by means of Density Functional Theory (DFT) calculations. Clusters containing up to six H atoms are investigated systematically – the clusters having either all H atoms on one side of the graphene sheet (*cis*-clusters) or having the H atoms on both sides in an alternating manner (*trans*-cluster). The most stable *cis*-clusters found have H atoms in ortho- and para-positions with respect to each other (two H's on neighboring or diagonally opposite carbon positions within one carbon hexagon) while the most stable *trans*-clusters found have H atoms in ortho-*trans*-positions with respect to each other (two H's on neighboring carbon positions, but on opposite sides of the graphene). Very stable *trans*-clusters with 13-22 H atoms were identified by optimizing the number of H atoms in ortho-*trans*-positions and thereby the number of closed, H-covered carbon hexagons. For the *cis*-clusters, the associative H₂ desorption was investigated. Generally, the desorption with the lowest activation energy proceeds via para-*cis*-dimer states, i.e. involving somewhere in the H clusters two H atoms that are positioned on opposite sites within one carbon hexagon. H₂ desorption from clusters lacking such H pairs is calculated to occur via hydrogen diffusion causing the formation of para-*cis*-dimer states. Studying the diffusion events showed a strong dependence of the diffusion energy barriers on the reaction energies and a general odd-even dependence on the number of H atoms in the *cis*-clusters.

I. INTRODUCTION

The interaction of H atoms and molecules with carbon based materials like graphite, single wall carbon nanotubes (SWCNT) and graphene has attracted considerable interest during the last two decades, since these systems are of interest in fields as diverse as astrochemistry, hydrogen storage and nanoelectronics.

The understanding of H chemisorption on graphitic materials and formation of H₂ molecules at low H atom densities is highly relevant for interstellar chemistry¹. H₂ formation in interstellar dust and molecular clouds is expected to occur via recombination of H atoms adsorbed on interstellar dust grain surfaces. Since carbonaceous grains are abundant in the interstellar medium, particular attention is focused on H chemisorption on graphite surfaces².

Most of the recent efforts regarding H adsorption on carbon-based materials have been stimulated by the possibility of using carbon nanostructures as a hydrogen storage medium³. Earlier reports on H storage of ~7.4 wt % in nanostructured graphite³ and 14 wt % in SWCNTs⁴ have not been confirmed by new experiments that rather indicate that the H storage capacity at room temperature is 3.8 wt % in graphite nanofibers⁵ and ~5.1 % in SWCNTs⁶. The precise mechanism of H adsorption in these structures is unknown since these values are well above the estimated limit of 1% for H₂ physisorption at room temperature⁷. For graphene a theoretical maximum storage capacity of 7.7 wt % is reported⁸.

Recent fabrication of graphene has generated an enormous number of new studies focused on the prospects of using graphene as a key material in post silicon

electronics^{9–11}. The high electron mobility can be exploited for construction of ballistic transistors operating at frequencies unreachable with current semiconductor materials¹². Yet, for applications in nanoelectronics efficient methods and tools for tailoring the electronic properties of graphene are required. One of the most promising routes towards the opening of a band gap in graphene is based on its hydrogenation^{8,13–15}. Hence, an atomic scale description of the binding mechanism and stability of small hydrogen structures formed on graphene will enhance efforts aimed at full control over graphene band gap engineering with deposited H atoms.

The chemisorption of H monomers on graphite has been studied extensively both experimentally and theoretically^{16–19}. H dimers on graphite or graphene have also been thoroughly studied in recent years^{19–26}. According to experiments, bigger structures will form when graphite or graphene are exposed to higher H doses^{14,15,21,27,28}. These structures, highly relevant for possible technological applications, are much less investigated than dimers. Only recently, Casolo *et al.*²⁴, Roman *et al.*²⁹, Ferro *et al.*³⁰ and Khazaei *et al.*³¹ used Density Functional Theory (DFT) to calculate the energetics of hydrogen clusters with three and four atoms, as well as one structure with six atoms on a graphene sheet. Cuppen *et al.*³² studied the formation of hydrogen clusters using Kinetic Monte Carlo methods. Luntz and co-workers³³ studied desorption of D₂ molecules from D clusters adsorbed on graphite, combining experimental and theoretical methods. A comprehensive list of tetramer structures and the recombination pathways was produced based on measured desorption density and DFT calculations³³. In the present paper we apply DFT to systematically study small hydrogen clus-

ters composed of three to six H atoms on graphene. Their structure and stability against H diffusion and H₂ recombination are determined at the atomic scale. Two types of clusters are considered, *cis*-clusters having all H atoms on the same side of the graphene sheet, and *trans*-clusters having the H atoms on both sides of the graphene sheet in an alternating manner. For the *trans*-clusters a few larger clusters were further considered. The computational method is described in Section II. The calculated H structures and their energetics are presented in Section III. The discussion of the results, including observed trends in the H binding with the size of H clusters, is given in Section IV. The results are summarized in Section V.

II. COMPUTATIONAL DETAILS

The DFT calculations were performed with the plane wave based DACAPO program package^{34,35}, applying ultra-soft pseudopotentials^{36,37} to describe electron-ion interactions, and the Perdew Wang functional (PW91) for the electronic exchange correlation effects. The electron wave functions and augmented electron density were expanded in plane waves with cutoff energies of 25 Ry and 140 Ry, respectively. The H cluster configurations were calculated by modelling the graphite surface with rhombohedral, periodically repeated slabs consisting of one graphene sheet having a 6×6 surface unit cell with 72 carbon atoms, and separated by 15 Å of vacuum. The Chadi-Cohen scheme³⁸ with six special points was used for sampling of the surface Brillouin zone. Binding energies of the n H clusters are reported per cluster using the clean graphene sheet plus n separate H atoms as the reference system, i.e.:

$$E_b = [E(\text{gra}) + nE(\text{H})] - E(n\text{H}/\text{gra}), \quad (1)$$

where $E(n\text{H}/\text{gra})$, $E(\text{gra})$ and $E(\text{H})$ are total energies of the n H clusters at graphene, the clean graphene sheet and the free H atom, respectively. The binding energies are well converged with respect to the number of **k**-points and the surface cell size as evidenced by Table I presenting the binding energies of the most favorable n H *cis*-clusters ($n \leq 6$) on graphene that we have encountered in the present investigation (i.e. the monomer, the orthodimer “O”, and trimers up to hexamers to be defined below). The H binding energy in gas-phase H₂ molecule calculated using computational method described above is 2.29 eV/H.

In figures 1-7 schematic illustrations of the H islands omitting the ionic relaxation patterns are shown. However, all structures were fully relaxed using the Broyden-Fletcher-Goldfarb-Shanno algorithm³⁹. The activation energies for diffusion of H atoms and for the H₂ recombination were calculated applying the nudged elastic band method⁴⁰ using at least seven configurations to model reaction paths. For sequences of reaction steps, we use the term *net barrier* to denote the energy difference between

Config.	# of H atoms	6×6 cell		7×7 cell	
		# of k -points	# of k -points	# of k -points	# of k -points
		6	18	6	18
monomer	1	0.77	0.81	0.78	0.82
O	2	2.73	2.76	2.73	2.75
H ₃ ^I	3	4.16	4.22	4.21	4.26
H ₄ ^I	4	6.27	6.32	6.28	6.29
H ₅ ^I	5	7.66	7.73	7.73	7.79
H ₆ ^I	6	9.62	9.68	9.66	9.69

TABLE I. Binding energies (in eV) of n H ($1 \leq n \leq 6$) *cis*-clusters adsorbed on graphene, as a function of the simulation cell size and the number of **k**-points used to sample the Brillouin zone. Results are given for the monomer, the orthodimer (“O”) and the most stable structures from Table III.

the initial state and the highest potential energy point along the path. This highest energy point will be a transition state of some n ’th reaction step along the path and the net barrier becomes the sum of the reaction energy for moving from the first initial state to the n ’th initial state *plus* the local barrier in the n ’th reaction step.

III. RESULTS

In the present paper we considered two types of adsorbed n H clusters: (A) *cis*-clusters with all H atoms adsorbed on the same side of the graphene sheet, and (B) *trans*-clusters where adsorbates bind at both sides of the graphene in an alternating manner. The corresponding results are presented in subsections III A and III B.

A. Cis-clusters: H adsorbed only on one side of the sheet

Since the activation energy of H diffusion through graphene is higher than 4 eV⁴¹ in the majority of experiments related to the H adsorption on graphite or graphene, the adsorbates will exclusively bind on the side of the graphene sheet exposed to the source of H atoms. Hence, we first consider this class of H configurations on graphene.

1. Hydrogen monomer and short dimers

The structure and binding energies of the H monomer and dimers have been studied by several groups^{18–20,24,26,42,43}. Our recent publication²⁶ contains well tested results for the H monomer and a comprehensive list of hydrogen dimer structures on graphene. The study includes H binding energies and activation energies of the most important kinetic processes. Since the results for bigger clusters presented in this paper will be compared to those of monomers and short dimers, for the sake of convenience we include in Fig. 1 and Table II

monomer		dimers	
config.	binding energy	config.	binding energy
monomer	0.77	O	2.73
		P	2.68
		M	1.58

TABLE II. Binding energies (in eV) of the monomer and short dimers at graphene²⁶.

relevant results of Ref.²⁶, calculated with the same computational set-up as used in the present study.

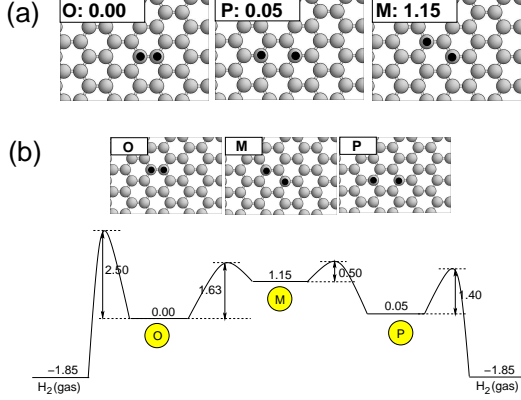


FIG. 1. (a) Three H short-dimer configurations on graphene. H and C atoms are represented with small black and gray spheres, respectively. Energies are given relative to the energy of the O-dimer structure; (b) the path and potential energy diagram for H_2 recombination from the O-dimer configuration. The transformation from the O-dimer to the P-dimer has a net barrier of 1.65 eV (the sum of 1.15 and 0.50 eV). All energies are in eV.

2. Hydrogen trimers

The trimer structures investigated in the present work are depicted in Figure 2(a), together with the total energies calculated relative to the energy of the H_3^I structure, identified as the most stable among the trimers considered. The binding energies of the H trimers are given in Table III. It is instructive to interpret the three most stable trimers (i.e. H_3^I , H_3^{II} and H_3^{III}) as being built from an ortho- or para-dimer (O- or P-dimer) with an extra atom added in an O- or a P-position. Adding the extra atom in a meta-position (M-position) results in less stable structures (i.e. H_3^{IV} and H_3^V). Thus the presence of an embedded M-dimer, i.e. involving somewhere in the H clusters two H atoms in M-position with respect to each other, appears to be strongly disfavored. The least stable trimers considered are triangular structures with the atoms in M- or extended dimer-positions (i.e. H_3^{VI} , H_3^{VII} and H_3^{VIII}).

The H_3^I and H_3^{III} structures were also presented by Casolo *et al.*²⁴, with the binding energies in very good

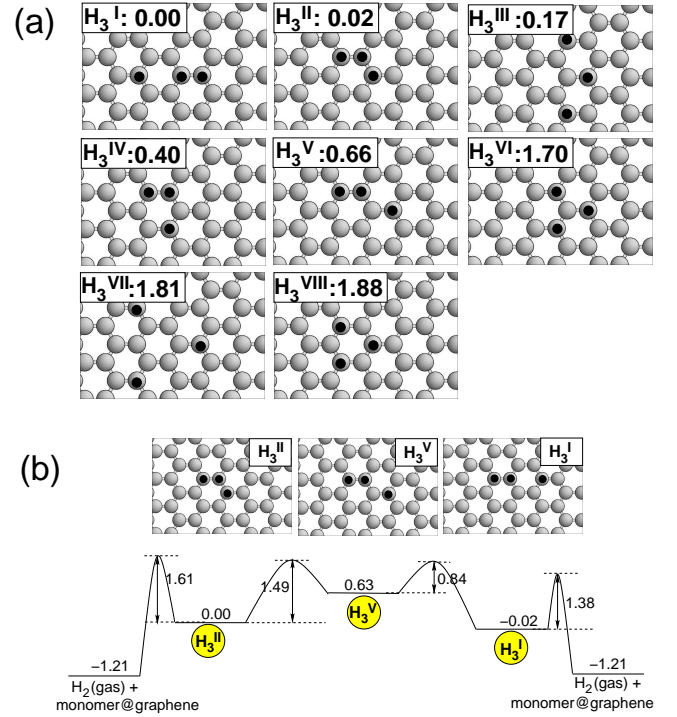


FIG. 2. (a) H trimer configurations on graphene. Energies are given relative to the energy of the H_3^I structure; (b) the paths and potential energy profiles for H_2 recombination from the H_3^I and H_3^{II} configurations. All energies are in eV.

agreement with the values reported here. The H_3^{VII} trimer was suggested by Khazaei *et al.*³¹ as a model for experimentally observed star like STM patterns, but appears as one of the least favorable trimer structures according to our work. Since we further calculate an energy barrier for H diffusion to neighbouring C sites of less than 0.65 eV for the H_3^{VII} configuration, it is unlikely to be stable at temperatures up to 600 K²⁷. A very comprehensive list of trimer structures is reported by Roman *et al.*²⁹. The most favorable structures (H_3^I , H_3^{II} and H_3^{III}) observed in the present work are in full agreement with the results in Ref.²⁹.

Considering the associative desorption of H_2 from the trimer structures we find that it occurs via an embedded P-dimer. The calculated pathways are sketched in Fig. 2(b) for the two most favorable structures (i.e. H_3^I and H_3^{II}). For configuration H_3^I that already contains an embedded P-dimer, the barrier is calculated to 1.38 eV, which is close to the one found for the isolated P-dimer (1.40 eV^{20,26} – see Fig. 1(b)). At the transition state along this pathway the H_2 molecule is nearly parallel to the surface with the H-H bond-length of ~ 1.2 Å. Very similar geometries of transition states are accounted for other reaction paths shown in Figs. 3 and 5. The H_3^{II} trimer does not contain an embedded P-dimer and the associative desorption from the embedded O-dimer is calculated to be associated with a barrier of 1.61 eV. An alternative scenario includes several H diffusion steps

trimers		tetramers		pentamers		hexamers	
config.	binding energy	config.	binding energy	config.	binding energy	config.	binding energy
H ₃ ^I	4.16	H ₄ ^I	6.27	H ₅ ^I	7.66	H ₆ ^I	9.62
H ₃ ^{II}	4.14	H ₄ ^{II}	6.10	H ₅ ^{II}	7.54	H ₆ ^{II}	9.57
H ₃ ^{III}	3.99	H ₄ ^{III}	6.06	H ₅ ^{III}	7.51	H ₆ ^{III}	9.55
H ₃ ^{IV}	3.76	H ₄ ^{IV}	6.05	H ₅ ^{IV}	7.50	H ₆ ^{IV}	9.42
H ₃ ^V	3.50	H ₄ ^V	5.94	H ₅ ^V	7.50	H ₆ ^V	9.31
H ₃ ^{VI}	2.46	H ₄ ^{VI}	5.87	H ₅ ^{VI}	7.49	H ₆ ^{VI}	9.27
H ₃ ^{VII}	2.35	H ₄ ^{VII}	5.85	H ₅ ^{VII}	7.47	H ₆ ^{VII}	9.23
H ₃ ^{VIII}	2.28	H ₄ ^{VIII}	5.51	H ₅ ^{VIII}	7.31	H ₆ ^{VIII}	9.21
		H ₄ ^{IX}	5.42	H ₅ ^{IX}	7.26	H ₆ ^{IX}	9.14
		H ₄ ^X	5.29	H ₅ ^X	7.25		
		H ₄ ^{XI}	5.20	H ₅ ^{XI}	7.24		
		H ₄ ^{XII}	5.12	H ₅ ^{XII}	7.15		
				H ₅ ^{XIII}	7.11		
				H ₅ ^{XIV}	7.09		

TABLE III. Binding energies (in eV) of n H cis-clusters at graphene. The cluster configurations are depicted in Figs. 2- 5.

transforming the H₃^{II} trimer via the H₃^V trimer to the H₃^I trimer for which the associative desorption can occur. Along this path, the highest activation energy becomes that of the transition from the H₃^{II} to the H₃^V trimer, which is 1.49 eV, see Fig. 2(b).

3. Hydrogen tetramers

The most favorable tetramer structures found are illustrated in Figure 3(a) and their binding energies are given in Table III. There are many low energy tetramers and a common feature for the very most stable of them (i.e. H₄^{I-VII}) seems to be that they are composed of one of the most stable trimers with an extra atom attached in an O- or a P-position. It is interesting to note that a triangular arrangement of the atoms seems to be particularly unfavorable. Comparing H₄^{XI} and H₄^{XII} one might guess based on the previous discussion that H₄^{XII} would be the more stable, since it contains exclusively atoms in P-positions, whereas in H₄^{XI} one atom is moved to a M-position. The same arguments apply when comparing H₄^{IX} and H₄^X. These triangular structures are unfavorable due to three H atoms adsorbed on the same C sublattice. Such imbalance in the occupation of two carbon sublattices creates additional unpaired electrons in the graphene lattice, increasing the total energy of the system. Note that for the trimers considered triangular structures were also very unfavorable. The pathways for H₂ recombination from the four most favorable configurations are depicted in Figure 3(b). As for the trimers, the recombination occurs from an embedded P-dimer, either directly [for the H₄^{II}, H₄^{III} and H₄^{IV} tetramers], or via H diffusion from the H₄^I over the H₄^{XIII} to the H₄^{III} structure, followed by H₂ associative desorption, as shown in Figure 3(b). The net barrier for H₂ formation from the H₄^I tetramer becomes 1.81 eV (the sum of 1.44 eV and 0.37 eV), which demonstrates a high stability of this con-

figuration. Other possible scenarios for H₂ recombination from tetramers are discussed in Ref.³³.

4. Hydrogen pentamers

The most stable pentamer structures in Figure 4 are formed by attachment of an additional H atom in an O- or a P-position to one of the preferential tetramer structures. The binding energies of the configurations considered are provided in Table III. The binding energies of the seven most stable structures are within an energy window of 0.2 eV. Although the other studied configurations are less favorable, the energy difference between the least (the H₅^{XIV}) and the overall most stable structure (the H₅^I) is smaller than 0.6 eV.

The activation energies for associative desorption are not calculated, since we expect that the H₂ formation occurs along pathways that are qualitatively similar to those of the tetramers, i.e. via direct associative recombination from embedded P-dimers or several steps of H diffusion between adjacent C sites, prior to the recombination from a P-dimer state.

5. Hydrogen hexamers

Hexamers are the largest H clusters considered systematically in the present study. In Fig. 5(a) the most stable structures identified are shown. The most favorable structure, H₆^I, has a total binding energy of 9.62 eV. Following the general trend outlined, the most stable hexamers contain motifs from stable smaller clusters and have all atoms in O- or P-positions. It is interesting to note that the H₆^I and the H₆^{II} structures have almost identical stability despite being quite different in geometry; the H₆^I is of low symmetry and has H atoms in O-positions while the H₆^{II} is of high symmetry and has

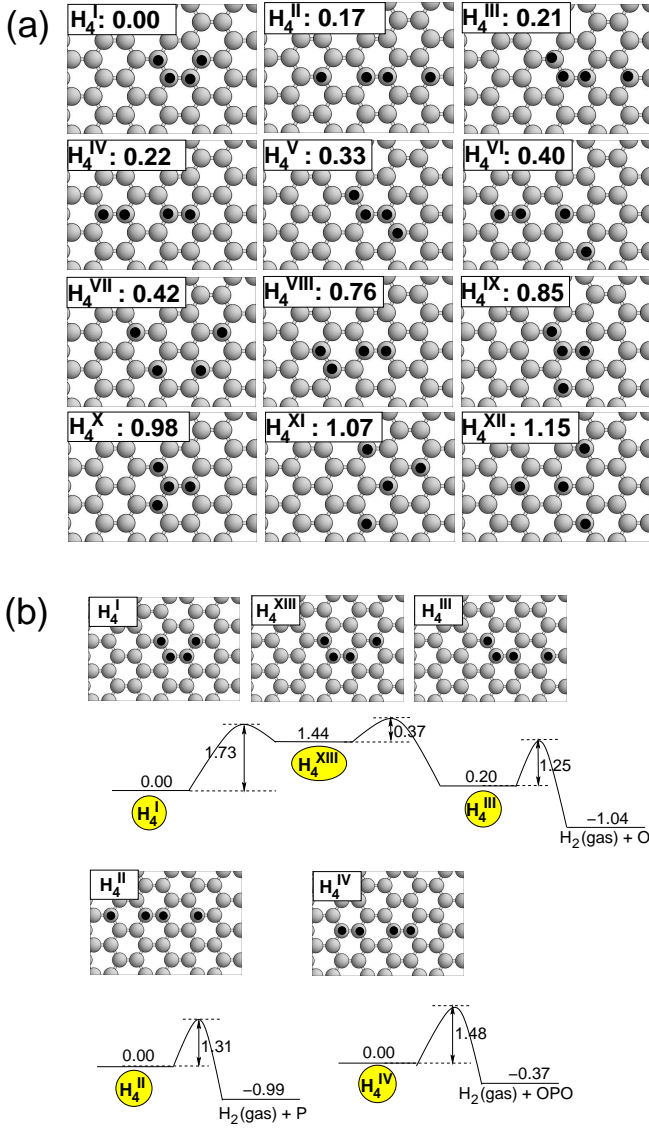


FIG. 3. (a) H tetramer configurations on graphene. Potential energies are given relative to the energy of the H_4^I structure. (b) The pathways for H_2 recombination from the H_4^I , H_4^{II} , H_4^{III} and H_4^{IV} configurations. The OPO is one of the long-dimer configurations from Ref.²⁶. All energies are in eV.

H atoms in P-positions. Generally, very many hexamer structures are found that differ only by a few tenths of an eV. For most of the structures presented in Fig. 5(a) the mechanism for the H_2 recombination and corresponding energy barriers are expected to be very similar to those determined for the dimers, trimers and tetramers. Thus, we did not perform the corresponding calculations. The reaction paths were however carefully calculated for the H_6^{II} and H_6^{VIII} structures, since both configurations possess ideal hexagonal symmetry. The breaking of the high symmetry of these two configurations might lead to activation energies for H_2 recombination that are higher than the typical values found for other H structures. The results for the H_2 formation from the H_6^{II} and H_6^{VIII}

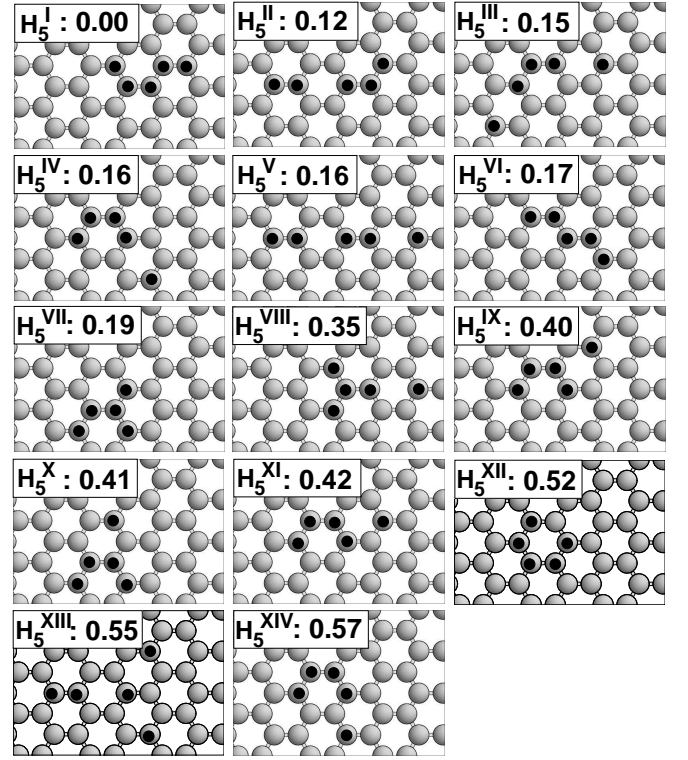


FIG. 4. H pentamer configurations on graphene. Potential energies (in eV) are given relative to the energy of the H_5^I structure.

hexamers are presented in Fig. 5(b). Indeed, the activation energies of 1.72 eV and 1.88 eV, calculated for H_6^{II} and H_6^{VIII} , respectively, indicate high kinetic stability of these structures with respect to molecular hydrogen formation. Ferro et al.³⁰ have suggested the H_6^{II} hexamer structure as a possible candidate for the experimentally observed very stable starlike STM patterns²⁷.

B. Trans-clusters: H adsorbed on both sides of the sheet

A common feature of the dimers in Ref.²⁶ and the cis-clusters presented in Figures 2 to 5 is that all H atoms are adsorbed on the same side of the graphene sheet. Given a very high energy barrier for H diffusion through the graphene layer this scenario is most likely to occur in defect-free samples deposited at crystalline surfaces. Yet, in free-standing graphene, graphene samples with defects or in small graphene patches, diffusion barriers at the defects or edges could be significantly lower than at the perfect sheet, opening routes for H adsorption on both sides of the layer. It turns out that such clusters – trans-clusters – are much more stable than those considered in the previous section. In the following, we present the results of our systematic investigation of trans-clusters with 2-6 H atoms, showing, however, only the very most stable structures identified. We further selectively chose

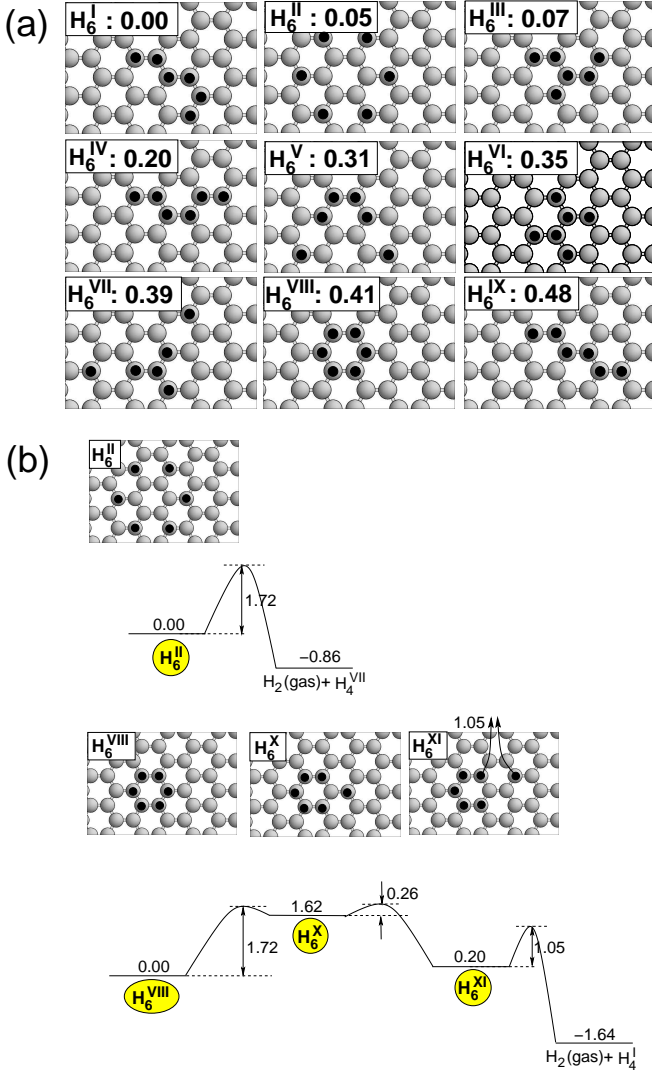


FIG. 5. (a) H hexamer configurations on graphene. Potential energies are given relative to the energy of H_6^I structure. (b) The reaction paths for H_2 recombination from the H_6^{II} and H_6^{VIII} configurations. All energies are in eV.

to study a few larger trans-clusters that will be presented and discussed.

The O-trans-dimer formed by adsorption of two H atoms in the configuration depicted in Fig. 6a is very stable with a total binding energy of 3.30 eV. This is by 0.54 eV higher than the binding in the O-dimer with the H atoms on the same side of the graphene sheet, i.e. the O-cis-dimer. The high stability of the O-trans-dimer configuration has already been reported by Roman *et al.*⁴⁴. The high stability of the O-trans-dimer appears to be related to the immediate proximity of the C atoms, since expanding the trans-dimer forming the *P-trans*- and *M-trans*-dimers of Fig. 6b and Fig. 6c leads to binding energies that are smaller by 0.79 and 1.82 eV, respectively, than that of the O-trans-dimer. In view of this finding, the search for the structures of the most stable larger H

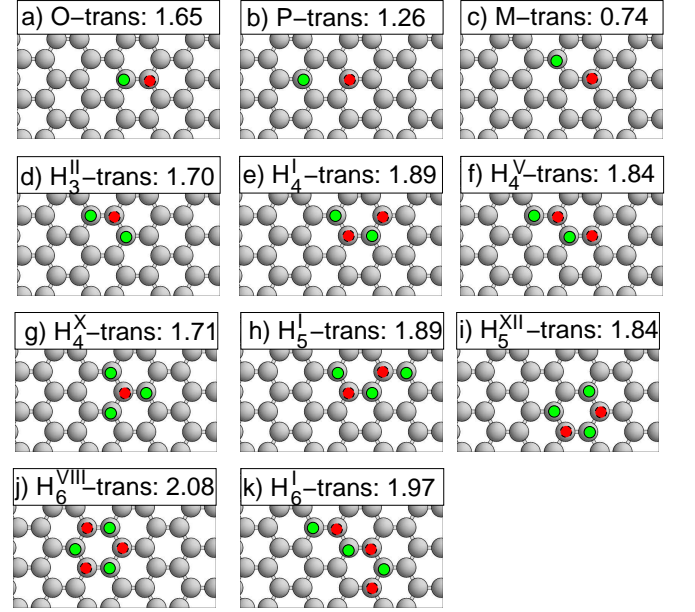


FIG. 6. H structures with atoms adsorbed on both sides of the graphene sheet: (a)-(c) trans-dimers; (d) trans-trimer; (e)-(g) trans-tetramers; (h)-(i) trans-pentamers; (j)-(k) trans-hexamers. Adatoms from opposite sides of the sheet are colored differently. Binding energies per H atom are given in eV.

clusters was limited to structures in which all neighboring H atoms were configured as in the O-trans-dimer.

The H_3^{II} -trans-trimer structure shown in Fig. 6d is the

configuration	# of H atoms	bind. energy (eV)	(eV/H)
O-trans [Fig. 6(a)]	2	3.30	1.65
P-trans [Fig. 6(b)]	2	2.51	1.26
M-trans [Fig. 6(c)]	2	1.48	0.74
H_3^{II} -trans [Fig. 6(d)]	3	5.11	1.70
H_4^I -trans [Fig. 6(e)]	4	7.56	1.89
H_4^V -trans [Fig. 6(f)]	4	7.36	1.84
H_4^X -trans [Fig. 6(g)]	4	6.83	1.71
H_5^I -trans [Fig. 6(h)]	5	9.44	1.89
H_5^{XII} -trans [Fig. 6(i)]	5	9.20	1.84
H_6^{VIII} -trans [Fig. 6(j)]	6	12.47	2.08
H_6^I -trans [Fig. 6(k)]	6	11.81	1.97

TABLE IV. Binding energies of hydrogen trans-clusters adsorbed on graphene.

most favorable trans-trimer structure found in our study. The binding energy of 5.11 eV, is by 0.89 eV higher than in the H_3^I cis-trimer.

Two almost equally stable trans-tetramers (H_4^I -trans and H_4^V -trans) were found as shown in Fig. 6e-f with binding energies of 7.56 and 7.36 eV. The triangular shaped trans-tetramer in Fig. 6g is slightly less stable with a binding energy of 6.83 eV, which is 0.73 eV smaller than Fig. 6e. This indicates that also for trans-clusters a triangular arrangement of the H atoms is disfavored,

and can in the same way as for the triangular shaped cis-clusters be related to an imbalance in the number of H atoms adsorbed on the two C sublattices. The most stable configuration, Fig. 6e, is as much as 1.26 eV more stable than the H_4^I -cis-tetramer in Fig. 3.

Two H trans-pentamers (H_5^I -trans and H_5^{XII} -trans) were investigated as shown in Fig. 6h and 6i. The calculated total H binding energies were 9.44 and 9.20 eV, respectively. The structure in Fig. 6h is by 1.71 eV more stable than the H_5^I -cis pentamer in Fig. 4.

The trans-hexamer in Fig. 6j (H_6^{VIII} -trans) is a particularly stable structure with a total binding energy of 12.47 eV which is 0.66 eV larger than that of the configuration in Fig. 6k (H_6^I -trans), and as much as 2.79 higher than the binding of the most stable cis-structure, H_6^I , in Fig. 5.

The graphane, fully hydrogenated graphene with hydrogen atoms adsorbed at carbon atoms on both sides of the sheet in an alternating manner^{8,14}, can be considered as the infinite trans-cluster. The H binding energy in graphane is 2.49 eV per atom, which is considerably more than the 2.08 eV calculated for the H_6^{VIII} -trans hexamer. Thus, with an increase in the size of trans-clusters we expect higher H binding energies, which should approach the value calculated for graphane. To examine this expected trend we considered several bigger trans-clusters. The larger trans-clusters considered are shown in Fig. 7. They have all been constructed as truncated pieces of graphane embedded in graphene. The most stable of the selected clusters are exclusively composed of closed hydrogenated carbon hexagons, already identified as the most stable small trans-clusters (H_6^{VIII} -trans). To further study the stability of these structures we included in our investigation configurations with missing H atoms on carbon hexagons at the cluster edges, which results in the occurrence of embedded M-dimers. Apart from the clusters having various sizes the primary difference is the configuration of the edge atoms. The H binding energies quoted in the figure do indeed increase with cluster size. This will be analyzed further in the Discussion Section.

C. Hydrogen induced magnetism

In a bipartite lattice, any imbalance in number of sites belonging to each of two sublattices leads to a magnetic ground state^{24,45,46}. One of the possible mechanisms to induce such an imbalance on graphene is adsorption of H atoms as has been discussed in the recent literature^{23,24,47,48}. According to our calculations, upon adsorption of a single H atom on graphene, small magnetic moments are observed at several C atoms in its vicinity. The calculated magnetic moments at the individual atoms are smaller than $0.1 \mu_B$. Concerning H dimers, non-zero spin density is observed only for structures with both hydrogens adsorbed on the C atoms from the same sublattice. According to the DFT calculations, these structures are unfavorable, and there-

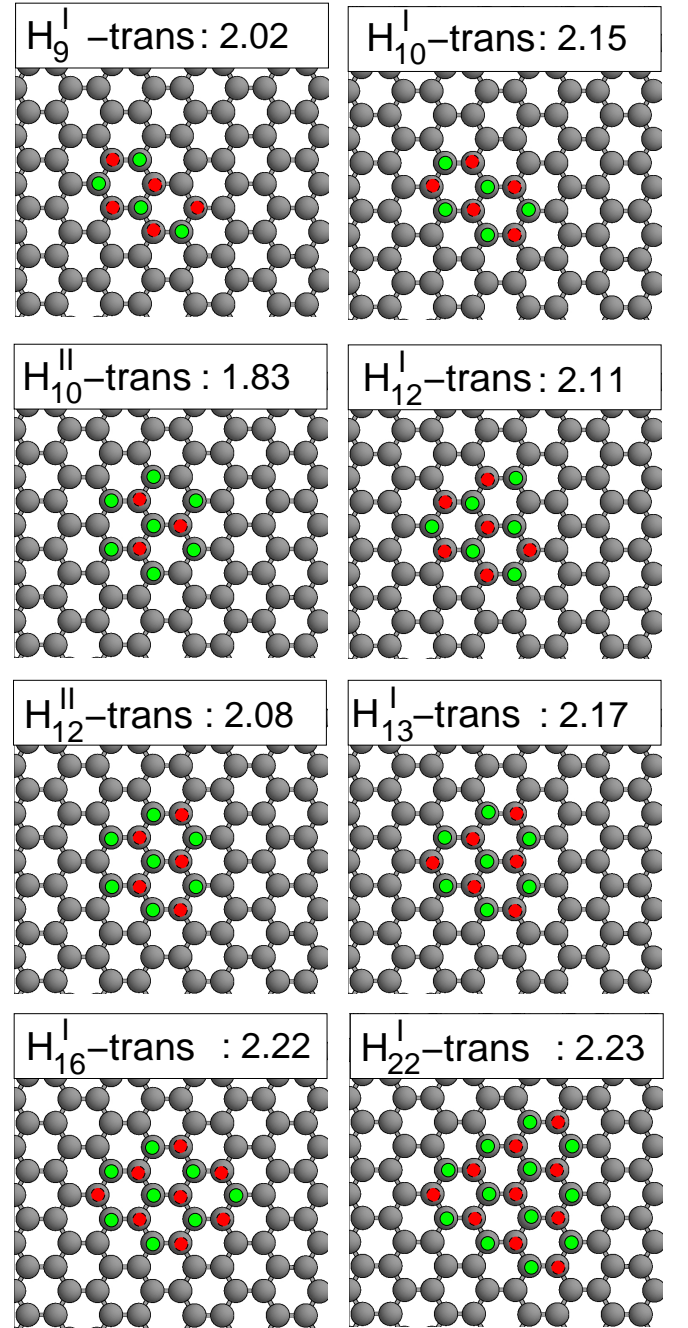


FIG. 7. Bigger H structures with atoms adsorbed on both sides of the graphene sheet. Adatoms from opposite sides of the sheet are colored differently. Binding energies per H atom are given in eV.

fore not expected to form in experiments. The energy gain due to spin-polarization does not affect the relative stability of the most favorable dimer structures obtained from non-spin-polarized calculations. This has already been demonstrated in our previous publication²⁶. A similar effect of the spin-polarization is found in the present work for the energetics of the investigated H cis configurations with three, four, five and six atoms.

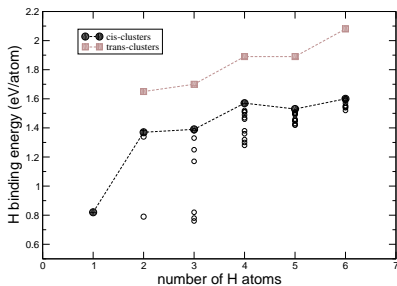


FIG. 8. The variation of the H binding energy with the size of cis- (circles) and trans-clusters (squares). The values corresponding to the most stable cis-structures (O-dimer, H_3^I -trimer, H_4^I -tetramer, H_5^I -pentamer and H_6^I -hexamer) are shown as big circles. Results for less stable cis-clusters from Tables II and III are given as small open circles.

However, several favorable trans-clusters investigated here (H_4^X -trans, H_{12}^{II} -trans, and H_{22}^I -trans) carry a total magnetic moment of $2 \mu_B$. We note that for these clusters, there is an imbalance between the number of H atoms on the two sides of the graphene sheet and that such graphene islands embedded in the graphene lend themselves as possible building blocks for graphene-based magnetic materials.

IV. DISCUSSION

The H adsorption on graphene in compact cis-cluster structures, described in Sec. III, is thermodynamically preferential compared to the adsorption of isolated H atoms. The binding energy of the H monomers is 0.77 eV. Already for the smallest clusters, such as O-dimers and H_3^I trimers the binding per H atom increases to 1.37 and 1.39 eV, respectively. The H binding in H_4^I tetramers is 1.57 eV, and slightly smaller in H_5^I pentamers, where we calculated binding energy of 1.53 eV per H atom. The strongest binding is evaluated for H_6^I hexamers, with the value of 1.60 eV per H atom. The evolution of the H binding energy with the size of the clusters is depicted by circles in Fig. 8.

If we consider the binding configurations in compact trans-cluster structures with H atoms adsorbed on both sides of the graphene sheet, Fig. 6, the trend in calculated values is similar: 1.65 eV (dimer), 1.7 eV (trimer), 1.89 eV (tetramer and pentamer), and 2.08 eV (hexamer). These binding energies are depicted by squares in Fig. 8 and are seen to be shifted to significantly higher values than in the clusters with H atoms adsorbed only on one side of the graphene sheet. Although our geometry for the O-trans dimer is slightly different from the one found by Boukhvalov *et al.*²⁵, their explanation of particularly favorable H adsorption on graphene observed in O-trans dimers is fully applicable to the clusters considered in this study. In Fig. 9a-b side views of the O-cis- and

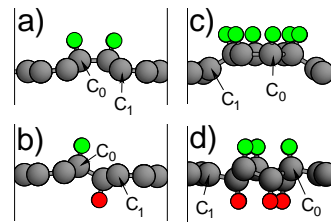


FIG. 9. The side views of (a) O-cis-dimer; (b) O-trans-dimer; (c) H_6^{VIII} -cis-hexamer; (d) H_6^{VIII} -trans-hexamer. The C atoms decorated with H are denoted as C_0 and their nearest neighbours without adsorbed H atoms as C_1 . Adatoms from opposite sides of the sheet are colored differently.

O-trans-dimers are shown and the carbon atoms are labeled. Using these labels, the H-C-C and C-C-C angles in the structures are given in Table V. From the Table it is seen that the angles calculated for trans-clusters are closer to the ideal tetrahedron value of 109.5° than those resulting for the cis-structures. Thus, in trans-clusters the H binding configurations allow creation of nearly perfect tetrahedral surroundings of C atoms directly involved in the interaction with adsorbates which results in an additional gain in the H chemisorption energy. An effect similar to that identified for the O-dimers is found when comparing the (H_6^{VIII} cis-hexamer [Fig. 5 and Fig. 9c] and the corresponding trans-hexamer structure [Fig. 6j and Fig. 9d] where all six C atoms from the hexagon decorated with H adatoms share favorable tetrahedral coordination. For bigger trans-clusters with fully hydrogenated carbon rings [H_{10}^I , H_{13}^I , H_{16}^I and H_{22}^I in Fig. 7] the H binding is further enhanced, slowly approaching the value encountered in graphane.

A similar investigation has not been carried out for cis-clusters since for this class of H adsorption configurations trends are less obvious. A full monolayer of H atoms can not be adsorbed on the same side of the graphene sheet. The maximum H coverage on graphene resulting in one or several stable adsorption configurations is also unknown. Thus, the trends in the structure and stability of bigger H cis-clusters on graphene is an open issue out of the scope of the present study.

A. Trends in stability of large trans-clusters

To rationalize the DFT results obtained for the big trans-clusters, Fig. 7, we construct in the following a simple model that reproduces the trends in stability of these clusters. In the model we identify closed hydrogenated carbon hexagons and a maximal ratio of inside atoms to edge atoms in the cluster as the most important structural motifs causing high cluster stability. On the other hand, removing a H atom from a closed hydrogenated carbon hexagon, i.e. introducing an embedded M-dimer, is modeled with an energy cost. Graphane, which can

	O-cis	O-trans		H8-cis	H8-trans
\angle H-C ₀ -C ₀	104.84	106.48	\angle H-C ₀ -C ₀	100.81	107.43
\angle H-C ₀ -C ₁	101.75	106.18	\angle H-C ₀ -C ₁	98.31	105.54
\angle C ₁ -C ₀ -C ₀	116.01	111.42	\angle C ₀ -C ₀ -C ₀	120.00	108.47
\angle C ₁ -C ₀ -C ₁	113.68	114.56	\angle C ₁ -C ₀ -C ₀	115.51	113.77

TABLE V. The angles (in deg.) calculated for dimers (O-cis and O-trans) and hexamers (H_6^{VIII} -cis and H_6^{VIII} -trans) in Fig. 9.

be considered as an infinite trans-cluster with no edge atoms, thus represents the highest achievable cluster stability.

In the model, the binding energy per H, $E(model)$, is defined as:

$$E(model) = (N_{inside}E_{inside}^B + N_{edge}E_{edge}^B - N_M E_M)/n. \quad (2)$$

where N_{inside} and N_{edge} are the number of inside and edge atoms, respectively and where N_M is the number of carbon sites where the lack of an H atom causes the appearance of an embedded M-dimer. The three energy terms, E_{inside}^B , E_{edge}^B , and E_M are fixed from calculated DFT values, i.e. they are not considered adjustable parameters. For E_{inside}^B we use 2.45 eV, which is the H-binding energy of graphane when the lattice constant of graphene, 1.42 Å is used (using the self-consistent graphane lattice constant of 1.46 Å it would be 2.49 eV). For E_{edge}^B we use 2.08 eV, which is the H binding energy of H_6^{VIII} -trans that has H atoms exclusively in edge sites. Finally, the energy penalty of introducing M-dimers, E_M , we extract from the calculated DFT energy difference between the E_6^{VIII} -trans and the E_5^{XII} -trans clusters [see Fig. 6], i.e. $E_M = 5 \cdot 2.08 - 5 \cdot 1.84 = 1.2$ eV.

For each of the clusters from Fig. 7 the relevant parameters and calculated energies are given in Table VI and Fig. 10. An excellent correlation between DFT val-

Config.	N_{inside}	N_{edge}	N_M	$E(model)$ (eV/H)	$E(DFT)$ (eV/H)
H_9^I	1	8	1	1.99	2.02
H_{10}^I	2	8	0	2.15	2.15
H_{10}^{II}	4	6	3	1.87	1.83
H_{12}^I	3	9	1	2.07	2.11
H_{12}^{II}	4	8	1	2.10	2.08
H_{13}^I	4	9	0	2.19	2.17
H_{16}^I	6	10	0	2.22	2.22
H_{22}^I	10	12	0	2.25	2.23

TABLE VI. The parameters and H binding energies from model, $E(model)$, and from the the full DFT calculations, $E(DFT)$.

ues for H binding in trans-clusters from Fig. 7 and the results obtained using Eq. 2 demonstrates that the general trends in the stability of graphene-like patches on graphene can be rationalized from the simple model with the parameters all determined by DFT calculations.

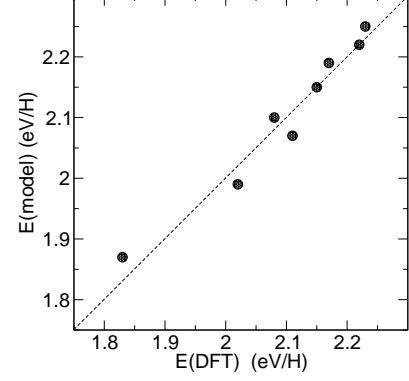


FIG. 10. The correlation between hydrogen binding energies for the clusters in Fig. 7, obtained from DFT calculations and those produced applying Eq. 2.

B. Trends in H diffusion barriers in cis-clusters

Even in the cis-structure with the highest H binding energy, i.e. the configuration H_6^I , the H binding energy is smaller than in the gas-phase H_2 molecule. Hence, all cis-clusters considered in the present study are metastable against associative H_2 desorption. Yet, at sufficiently low temperatures this process will be hindered due to the considerable activation energies that we calculate. According to our previous studies^{20,26} the lowest activation energy for H_2 recombination from H dimers is calculated for the P-dimer state. In other dimer structures and for many of the large H clusters, the recombination includes one or several diffusion steps of H atoms leading to the formation of the embedded P-dimer, followed by the H_2 associative desorption.

To lay the grounds for understanding these events, we performed a comprehensive set of calculations regarding energy barriers for H diffusion on graphene, considering most of the structures presented in Figs. 3-5. According to the universality concept of Nørskov and co-workers^{49,50}, the activation energies for diffusion of atoms on (metal) surfaces correlate with the differences between their binding energies in the initial and final states. Correlation diagrams—so-called Brønsted-Evans-Polanyi (BEP) plots—reveal that weaker bound adsorbates generally diffuse with lower activation energies. The BEP plot in Fig. 11 clearly demonstrates this trend for H diffusion at graphene. The barrier for diffusion of an isolated H atom ($\Delta E=0$) is 1.14 eV. However, the barrier vanishes if the final state is by ~ 2 eV more favorable than the initial

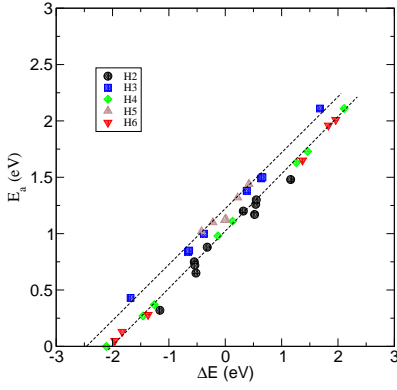


FIG. 11. Brønsted-Evans-Polanyi plot for selected H *cis*-clusters from Figures 2-5. For each of the considered H clusters we calculated the energy barrier (E_a) for H diffusion to one of nearest non-hydrogenated C sites. ΔE is a difference in total energies of a cluster configuration produced upon H diffusion and the initial one. The dashed lines represent corresponding linear relations between E_a and ΔE for structures with odd and even number of H atoms given by Eq. 3.

one, or increases above 2 eV for diffusion in the opposite direction. For most of the configurations investigated in the present study the activation energies for diffusion of atomic H are in the range from 0.7 to 1.5 eV. Applying the linear least square fitting to the DFT values calculated for E_a (the activation energy for H atom diffusion between adjacent C sites) and ΔE (the energy difference between configurations after and prior to H diffusion), we arrive at the following expressions for clusters with n H atoms:

$$E_a(n) = \begin{cases} 1.0 \text{ eV} + 0.5\Delta E, & n \text{ even} \\ 1.2 \text{ eV} + 0.5\Delta E, & n \text{ odd.} \end{cases} \quad (3)$$

We did not find clear arguments for observed energy shift of 0.2 eV in the E_a between configurations with even (dimers, tetramers and hexamers) and odd (trimers and pentamers) number of H atoms. Yet, Eq. 3 and the BEP plot in Fig. 11 demonstrate that for H structures

on graphene a fairly accurate estimate of their stability against H diffusion can be obtained from total energies of initial and final states, without explicit calculation of the corresponding activation energy E_a .

V. CONCLUSIONS

We investigated an extensive set of adsorption configurations of H atom clusters on graphene, the H atoms being either all on one side of the graphene (*cis*-clusters) or on both sides in an alternating manner (*trans*-clusters). The binding energy per H atom in general increases with the size of the clusters. The value of 0.77, calculated for monomers, increases to 1.6 eV in *cis*-hexamers and to 2.08 eV in *trans*-hexamers. H-H interactions appear to favor *cis*-cluster shapes having H atoms in O- and P-positions with respect to each other and to favor *trans*-clusters having H atoms in O-positions with respect to each other. Very stable *trans*-clusters with 13-22 H atoms were identified by optimizing the number of H atoms in ortho-*trans*-positions and thereby the number of closed, H-covered carbon hexagons. For such clusters, H binding energies up to 2.23 eV were found. For the *cis*-clusters, associative H_2 desorption was investigated. It was found that desorption occurred from P-dimers embedded in the clusters or from pairs of H atoms that first rearranged via diffusion into embedded P-dimers, with barriers ranging from ~ 1.4 to ~ 1.7 eV. Upon formation of clusters with an odd number of adsorbates a non-zero spin-density is induced. However, for the most stable *cis*-configurations the spin-polarization is rather weak. The most stable *cis*-configurations with an even number of H atoms are all non-magnetic. Yet, some of the very stable *trans*-clusters are magnetic, which opens routes for design of magnetic materials based on graphene functionalized with hydrogen.

This work has been supported by the Serbian Ministry of Science and Technological Development under Grant No. 141039A and by the Danish Research Councils. The calculations were performed at the Danish Center for Scientific Computing.

¹ *The Molecular Astrophysics of Stars and Galaxies*, ed. by T. W. Hartquist and D. A. Williams, (Clarendon, Oxford, 1999).

² S. Cazaux and A. Tielens, *Astrophys. J.* **604**, 222 (2004).

³ L. Schlapbach and A. Züttel, *Nature* **414**, 353 (2001).

⁴ A. C. Dillon and M. J. Heben, *Appl. Phys. A: Matter. Sci. Process.* **72**, 133 (2001).

⁵ A. d. Lueking, R. T. Yang, N. M. Rodriguez and R. T. K. Baker, *Langmuir* **20**, 714 (2004).

⁶ A. Nikitin, H. Ogasawara, D. Mann, R. Denecke, Z. Zhang, H. Dai, K. Cho and A. Nilsson, *Phys. Rev. Lett.* **95**, 225507 (2005).

⁷ M. Ritschel, M. Uhlemann, O. Gutfleisch, A. Leonhardt, A. Graff, Ch. Täschner and J. Fink, *Appl. Phys. Lett.* **80**, 2985 (2002).

⁸ J. O. Sofo, A. S. Chaudhari and G. D. Barber, *Phys. Rev. B* **75**, 153401 (2007).

⁹ K. S. Novoselov, A. K. Geim, S. V. Morozov, D. Jiang, M. I. Katsnelson, I. V. Grigorieva, S. V. Dubonos, A. A. Firsov, *Nature* **438**, 197 (2005).

¹⁰ A. K. Geim and K. S. Novoselov, *Nat. Mat.* **6**, 183 (2007).

¹¹ A. H. Castro Neto, F. Guinea, N. M. R. Peres, NMR, K. S. Novoselov, and A. K. Geim, *Rev. Mod. Phys.* **81**, 109 (2009).

- ¹² Y. -M. Lin, C. Dimitrakopoulos, K. A. Jenkins, D. B. Farmer, H. -Y. Chiu, A. Grill and Ph. Avouris, *Science* **327**, 662 (2010).
- ¹³ E. J. Duplock, M. Scheffler and P. J. D. Lindan, *Phys. Rev. Lett.* **92**, 225502, 2004.
- ¹⁴ D. C. Elias, R. R. Nair, T. M. G. Mohiuddin, S. V. Morozov, P. Blake, M. P. Halsall, A. C. Ferrari, D. W. Boukhvalov, M. I. Katsnelson, A. K. Geim, K. S. Novoselov, *Science* **323**, 610 (2009).
- ¹⁵ R. Balog, B. Jorgensen, L. Nilsson, M. Andersen, E. Rienks E, M. Bianchi, M. Fanetti, E. Laegsgaard, A. Baraldi A, S. Lizzit, Z. Šljivančanin, F. Besenbacher, B. Hammer, T. G. Pedersen, P. Hofmann and L. Hornekær, *Nat. Mat.* **9**, 315 (2010).
- ¹⁶ D. Neumann, G. Meister, U. Kurpick, A. Goldmann, J. Roth and V. Dose, *Appl. Phys. A* **55**, 489 (1992).
- ¹⁷ L. Jelaica and V. Sidis, *Chem. Phys. Lett.* **300**, 157 (1999).
- ¹⁸ X. Sha and B. Jackson, *Surface Science* **496**, 318 (2002).
- ¹⁹ T. Zecho, A. Güttler, X. Sha, B. Jackson and J. Küppers, *J. Chem. Phys.* **117**, 8486 (2002).
- ²⁰ L. Hornekær, Ž. Šljivančanin, W. Xu, R. Otero, E. Rauls, I. Stensgaard, E. Lægsgaard, B. Hammer and F. Besenbacher, *Phys. Rev. Lett.* **96**, 156104 (2006).
- ²¹ L. Hornekær, E. Rauls, W. Xu, Ž. Šljivančanin, R. Otero, I. Steensgaard, E. Lægsgaard, B. Hammer and F. Besenbacher, *Phys. Rev. Lett.* **97**, 186102 (2006).
- ²² T. Roman, W. Dinö, H. Nakanishi, H. Kasai, T. Sugimoto and K. Tange, *Carbon* **45**, 203 (2007).
- ²³ Y. Ferro, D. Teillet-Billy, N. Rougeau, V. Sidis, S. Morisset, and A. Allouche, *Phys. Rev. B* **78** (2008) 085417.
- ²⁴ S. Casolo, O. M. Løvik, R. Martinazzo and G. F. Tantarini, *J. Chem. Phys.* **130**, 054704 (2009).
- ²⁵ D. W. Boukhvalov, M. I. Katsnelson and A. I. Lichtenstein, *Phys. Rev. B* **77**, 035427 (2008).
- ²⁶ Ž. Šljivančanin, E. Rauls, L. Hornekær, W. Xu, F. Besenbacher and B. Hammer, *J. Chem. Phys.* **131**, 084706 (2009).
- ²⁷ L. Hornekær, W. Xu, R. Otero, E. Laegsgaard and F. Besenbacher, *Chem. Phys. Lett.* **446**, 237 (2007).
- ²⁸ R. Balog, B. Jørgensen, J. Wells, E. Lægsgaard, P. Hofmann, F. Besenbacher and L. Hornekær, *J. Am. Chem. Soc.* **131**, 8744 (2009).
- ²⁹ T. Roman, H. Nakanishi, H. Kasai, H. Nobuhare, T. Sugimoto and K. Tange, *J. Phys. Soc. Japan* **78**, 035002 (2009).
- ³⁰ Y. Ferro, S. Morisset, A. Allouche, *Chem. Phys. Lett.* **478**, 42 (2009).
- ³¹ M. Khazaei, M. S. Bahrany, A. Ranjbar, H. Mizuseki and Y. Kawazoe, *Carbon* **47**, 3306 (2009).
- ³² H. Cuppen and L. Hornekær, *J. Chem. Phys.* **128**, 174707 (2008).
- ³³ S. Baouche, L. Hornekær, A. Baurichter, A. C. Luntz, V. V. Petrunin and Ž. Šljivančanin, *J. Chem. Phys.* **131**, 244707 (2009).
- ³⁴ B. Hammer, L. B. Hansen, J. K. Nørskov, *Phys. Rev. B* **59**, 7413 (1999).
- ³⁵ S. R. Bahn, K. W. Jacobsen, *Comput. Sci. Eng.* **4**, 56 (2002).
- ³⁶ D. Vanderbilt, *Phys. Rev. B* **41**, R7892 (1990).
- ³⁷ K. Laasonen, A. Pasquarello, R. Car, C. Lee, D. Vanderbilt, *Phys. Rev. B* **47**, 10142 (1993).
- ³⁸ D. J. Chadi, M. L. Cohen, *Phys. Rev. B* **8**, 5747 (1973).
- ³⁹ D. C. Liu and J. Nocedal, *Math. Program.* **45**, 503 (1989).
- ⁴⁰ H. Jónsson, G. Mills and K. W. Jacobsen, in *Classical and Quantum Dynamics in Condensed Phase Simulations*, ed. by B. J. Berne, G. Ciccoti, and D. F. Coker, (World Scientific, Singapore, 1998).
- ⁴¹ Y. Ferro, F. Marinelli and A. Allouche, *J. Chem. Phys.* **116**, 8124 (2002).
- ⁴² Y. Ferro, F. Marinelli and A. Allouche, *Chem. Phys. Lett.* **368**, 609 (2003).
- ⁴³ Y. Miura, H. Kasai, W. Dino, H. Nakanishi and T. Sugimoto, *J. Appl. Phys.* **93**, 3395 (2003).
- ⁴⁴ T. Roman, W. A. Dino, H. Nakanishi, and H. Kasai, *J. Phys. Condens. Mat.* **21**, 474219 (2009).
- ⁴⁵ E. H. Lieb, *Phys. Rev. Lett.* **62**, 1201 (1989).
- ⁴⁶ J. A. Verges and P. L. de Andres, *Phys. Rev. B* **81**, 075423 (2010).
- ⁴⁷ O. V. Yazyev, L. Helm, *Phys. Rev. B* **75**, 125408 (2007).
- ⁴⁸ Y. Lei, S. A. Shevlin, W. Zhu and Z. X. Guo, *Phys. Rev. B* **77**, 134114 (2008).
- ⁴⁹ J. K. Nørskov, T. Bligaard, A. Logadottir, S. Bahn, L. B. Hansen, M. Bollinger, H. Bengaard, B. Hammer, Ž. Šljivančanin, M. Mavrikakis, Y. Xu, S. Dahl and C. J. H. Jacobsen, *J. Catal.* **209**, 275 (2002).
- ⁵⁰ B. Hammer, *Topics in Catal.* **37**, 3 (2006).